# MULTI-OBJECTIVE GENETIC OPTIMIZATION FOR LCLSII X-RAY FEL[†]

L. Wang[#] and T. O. Raubenheimer, SLAC, Menlo Park, CA, USA

## Abstract

The Linac Coherent Light Source II (LCLS-II) will build on the success of the world's most powerful X-ray laser, the Linac Coherent Light Source (LCLS). It will add two new X-ray laser beams and room for additional new instruments, greatly increasing the number of experiments carried out each year. Multiple operation modes are proposed to accommodate a variety of user requirements. There are a large number of variables and objectives in the design. For each operation mode, Multi-Objective Genetic Algorithm (MOGA) is applied to optimize the machine parameters in order to minimize the jitters, energy spread, collective effects and emittance.

## INTRODUCTION

LCLS-II will provide beam with difference charge. For each beam, the bunch compressors, R56 at BC1 and BC2, accelerating structure phase and voltage are optimized using MOGA program to satisfy the required peak current, and to minimize the energy spread, energy chirp, current jitter, energy jitter and time jitter. We briefly summarize the MOGA optimization for LCLS, LCLSII and the two beam configuration.

The transverse emittance growth due to CSR is minimized by choosing appropriate phase advance between BC2 and the downstream bending magnets. The final emittance at the beginning of the undulator is just about 1um and even lower for low charge.

## BENCHMARK WITH LCLS BEAM

It is important to have a comparision of the simulation with the measurements. A series of data, for instance, the voltage and phase of Linac 1and 2, energy at BC1, BC2 and DL2, beam current at BC1 and BC2, were taken at the LCLS to set-up the variations and then compare the jitters in beam current and energy. One example of the variation of L2 voltage and DL2 energy are shown in Fig. 1. We uses these varations to study the enegy and beam current jitter. The main machine parameters used in the simulation are listed in Table 1 as oeprational model. The values of these parameters are not exactly the same as the readings from MCC. Some parameters, especially the phase of RF, are tweaked to get flat top current profile and zero energy chirp at the beginning tof the undulator similar to the measured values. The bunch charge is 150 pC. FIG.2 shows the bunch profile before the undulator by LiTrack simulation, which gives a simliar bunch current ~ 3kA. The measured energy jitter in the machine is about 0.049%, which is slighly larger than the the simulation result of 0.033%. The L0 jitter is not included in the simulation since the simulation starts after L0 and this will cause the simulated jitter to be low [1].

The main contributions of the energy jitters in the operational mode are L1 phase and voltage, LX phase and L2 phase. One of the optmized configurations is also listed in Table 1. This optmized configuration reduces the energy jitter by a factor 2. Fig.3 shows the comparision of the energy jitter for the optmized mode and the operational one. There are large reductions for the four major contributions. The energy jitter of the optimized mode is widely distributed compared with the operational mode. It clearly shows the benefit from optmization. We are doing detail benchmark with the measurement: taking the OTR4 phase space data as the input of the simulation and comparing the phase space in the middle of BC1, BC2 and DL2. New features are being added to Litrack code for such comparision.
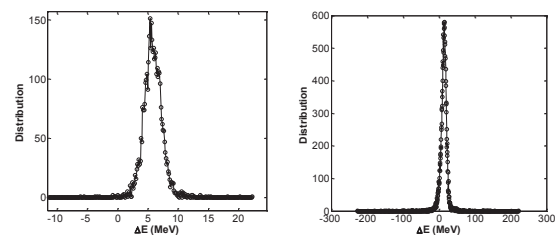


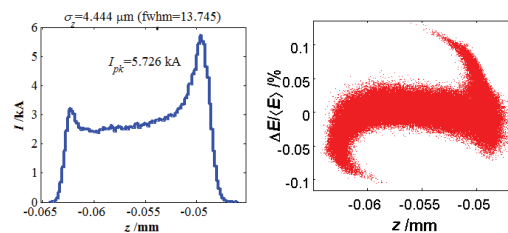Figure 1: Variation of the L2 voltage and DL2 energy at LCLS.



Figure 2: The bunch profile and phase space at the beginning of the undulator for 150pC beam at LCLS. Bunch head is on the left.

Table 1: Example of LCLS operational and optimized model.

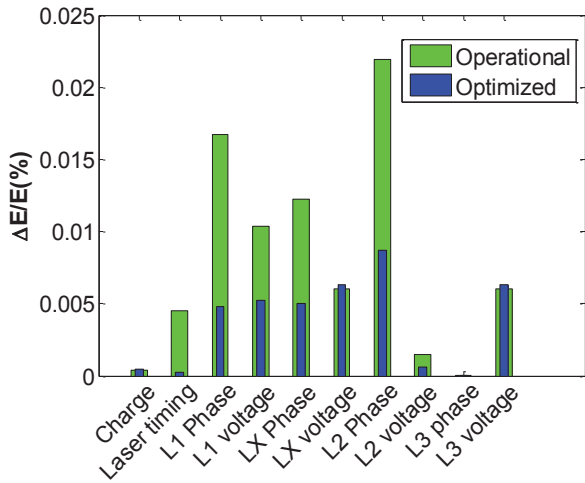| Variables | optimized | ~operational |
|---|---|---|
| $I_{pk}$ (kA) | 3 | 3 |
| $\phi_{L1}$ (degree) | -19.3 | -26.1 |
| $V_{L1}$(MV) | 111 | 118 |
| $\phi_{Lx}$ (degree) | -154 | -160 |
| $V_{Lx}$(MV) | 22 | 22 |
| $\phi_{L2}$ (degree) | -19 | -38.7 |
| $V_{L2}$(GV) | 5.06 | 6.15 |
| $\phi_{L3}$ (degree) | -10.3 | 0 |
| $V_{L3}$(GV) | 8.79 | 7.667 |
| $R_{56}$@BC1(mm) | -45.5 | -45.5 |
| $R_{56}$@BC2(mm) | -51.3 | -20.6 |
| $(\Delta I/I)$ (%) | 10 | 7 |
| $(\Delta E/E)$ (%) | 0.014 | 0.033 |

Figure 3: Comparison of the distribution of energy jitters for the operational mode and optimized one.

## OPTMIZATION OF LCLSII

Fig. 4 shows the layout of LCLSII design. The energy at the Bunch Compressor 1 (BC1) and 2 (BC2) is 335 MeV and 4.5 GeV, respectively. The Gun simulation is done using IMPACT. The Litrack code is used to study the longitudinal dynamics from L0 to the beginning of undulator. There are total 10 variables in the optimization: the phases and voltages of Linac 1(L1), X-band Linac (LX), Linac 2 (L2), Linac 3 (L3), $R_{56}$ at BC1 and BC2. The constraints include the energies at BC1, BC2 and beginning of the undulator, the cancellation of quadratic energy chirp with X-band structure, and a peak current of 3.0 kA or 4.0 kA at the end of beam line. For each bunch charge mode, we need to minimize the energy spread, linear energy chirp, peak current jitter, energy jitter and timing jitter. All these jitters are normalized and added together according to their weights to get a single objective. In most of the optimization, we set an equal weight for them. The resistive wall wake of the chamber and the wake field of the accelerating structures are also included in the simulation.

The optimization is done for each bunch charge. Table 2 shows the example of the solutions for 250 pC and 150 pC cases. These solutions have smaller timing and energy jitters than required for SASE operation while the current the jitter is close to the requirement of 12%. In the optimization, an equal weight is used for energy, current and timing jitters. We can set a larger weight for the current jitter to reduce the current jitter, if desired.

Fig. 5 shows the phase space along the beam line for 250 $pC$ case. It clearly shows a non-zero energy chirp at the end of the linac (L3) and the subsequent reduction of the chirp before the undulator due to the wake field effect. Fig. 6 shows the current profile of 150pC case. There is a double horn in the beam profile due to the effect of nonlinear wake field. Fig. 7 shows the distribution of the jitters for 250 pC case. The variations (errors) used for the jitter study are listed in Table 3. The jitters are widely distributed, especially for the energy jitter. The current

jitter is dominant by the effect of LX phase, L2 phase and L1 voltage, the timing jitter is not an issue. The energy jitter is important for the seeding FEL in LCLS. An energy jitter of 0.042%, which is close to the measured energy jitter in LCLS, reduces the FEL intensity to 70% of the peak value. If the energy jitter can be reduced to 0.02%, the FEL intensity will be 90% of the peak. We are working to minimize the energy jitter in various ways, including MOGA optimization.
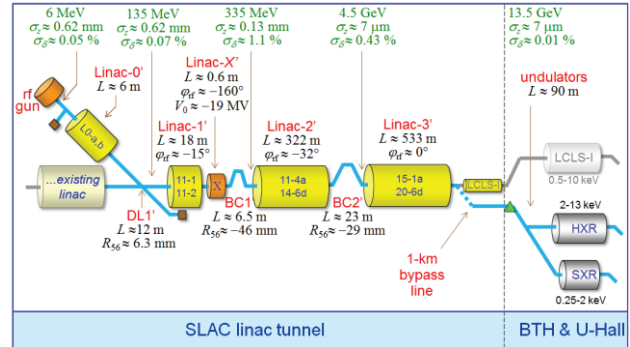


Figure 4: Layout of LCLSII.

Table 2: Configurations and jitters of different bunch charge.

| Variables | 250pC | 150pC |
|---|---|---|
| $I_{pk}$ (kA) | 3 | 3 |
| $\phi_{L1}$ (degree) | -26 | -24 |
| $V_{L1}$(MV) | 262 | 248 |
| $\phi_{Lx}$ (degree) | -165 | -168 |
| $V_{Lx}$(MV) | 38 | 29 |
| $\phi_{L2}$ (degree) | -38 | -36 |
| $V_{L2}$(GV) | 5.26 | 5.16 |
| $\phi_{L3}$ (degree) | -4 | -3 |
| $V_{L3}$(GV) | 9.06 | 9.04 |
| $R_{56}$@BC1(mm) | -30 | -38 |
| $R_{56}$@BC2(mm) | -22 | -23 |
| $\sigma_E/E$ (%) | 0.013 | 0.013 |
| $(\Delta I/I)$ (%) | 9 | 14 |
| $(\Delta E/E)$ (%) | 0.039 | 0.038 |
| $(\Delta\tau)$ (fs) | 49 | 51 |

Table 3: The tolerence used for evaulation of the jitters.

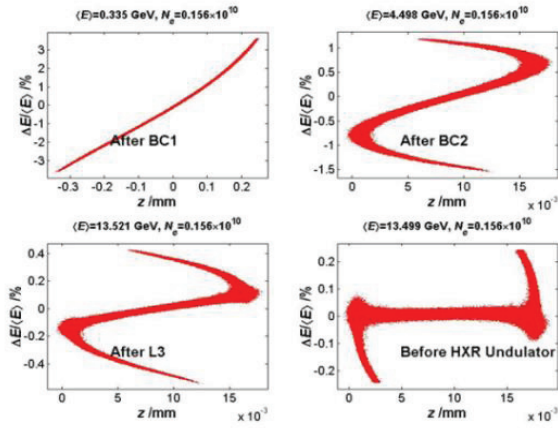| | Symbol | errors |
|---|---|---|
| Relative Bunch Charge | $\Delta Q/Q$ | 1% |
| Driven Laser timing | $\Delta\tau$ | 0.2ps |
| L1 RF Phase | $\Delta\varphi_1$ | 0.05° |
| LX RF Phase | $\Delta\varphi_x$ | 0.3° |
| L2 RF Phase | $\Delta\varphi_2$ | 0.04° |
| L3 RF phase | $\Delta\varphi_3$ | 0.03° |
| L1 RF relative voltage | $\Delta V/V_1$ | 0.05% |
| LX RF relative voltage | $\Delta V/V_x$ | 0.25% |
| L2 RF relative voltage | $\Delta V/V_2$ | 0.05% |
| L3 RF relative voltage | $\Delta V/V_3$ | 0.02% |

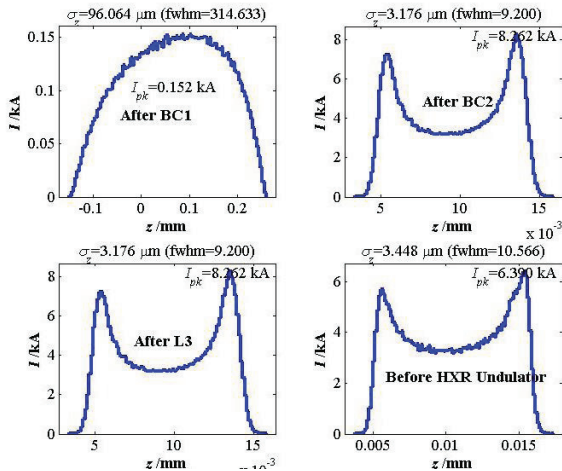Figure 5: Example of phase space for 250pC Hard X-ray.



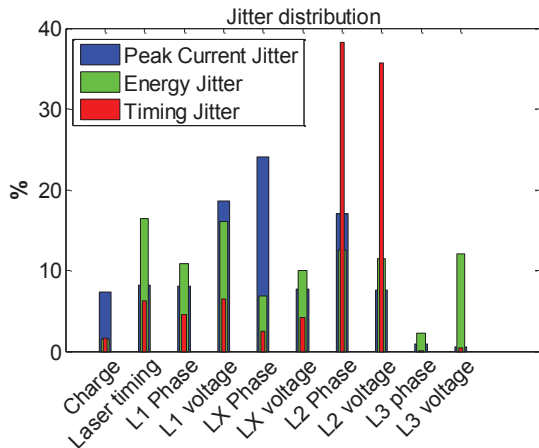Figure 6. Example of beam profile for 150pC Hard X-ray.



Figure 7: Distributions of the Jitters for 250 pC hard X-ray configuration.



Figure 8: Sketch of LCLSII+, a two beam energy FEL machine beyond LCLSII.

# LCLSII+, TWO BEAM ENERGY MACHINE

We present one potential upgrade to the LCLSII design, referred to as LCLSII+. This option integrates LCLS and LCLSII together to provide two simultaneous beam energies at a 360Hz repetition rate. Fig. 8 shows the sketch of LCSII+. The LCLSII linac, operated at 360 Hz, can provide low energy beam, for instance 7.5 GeV. Some low energy bunches (after L3) are kicked to the LCLSII by-pass beam line to radiate directly. The rest of the low energy bunches are continuously accelerated and compressed along the existing LCLS accelerator to achieve an energy above 16 GeV. The first bunch compressor in LCLS is replaced by a bunch lengthener (BL) to increase the bunch length in order to increase the energy chirp and also reduce the effect of wake field. The combination of BL and BC3 provide the flexibility to adjust the bunch current/profile of the high energy beam. A wake field type of de-chirper could be added fin the Bypass line as an option to control the final energy chirp. It is not used in this design.

To increase the repetition rate from current 120 *Hz* to 360 *Hz*, the maximum accelerating gradient is lower by a factor of ~1.8. Therefore, a longer accelerating structure is needed to get the same beam energy. The existing S-band accelerating structure is assumed for 360 *Hz* repetition rate. X-band can be chosen for even high repetition rate. However, the stronger wake field may limit the flexibility to achieve desired beam and it is also expensive.

It is import to study the flexibility to provide the two simultaneous beams with good beam quality, such as high peak current with small energy spread, for different charges. Fig. 9 shows the example of 150 pC bunch charge case. Both beams have high peak current, above 3 *kA,* and small energy chirp. A small positive energy chirp is intentionally kept for the low energy beam, which can be easily adjusted by the adjusting the RF phases. There are small R56 of 3.5 *mm* at BL and -7.5 *mm* at BC3. The peak current can be easily adjusted by the change of R56 at BC3 and BL.

Fig. 10 shows the 20 pC charge case. The R56 is 2.5 mm and -6.0 mm at BL and BC3, respectively. Again, there is large flexibility to adjust the peak current of the high energy beam. The peak current is about 4kA in the example. The energy chirps for both beams are about zero. Study shows that high bunch charge 250 pC also works well. The large flexibilities of this two energy scheme with high repetition rate of 360 *Hz* make this type of machine very attractive.
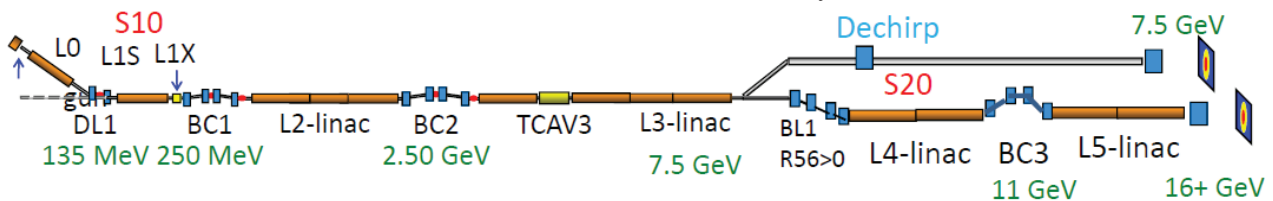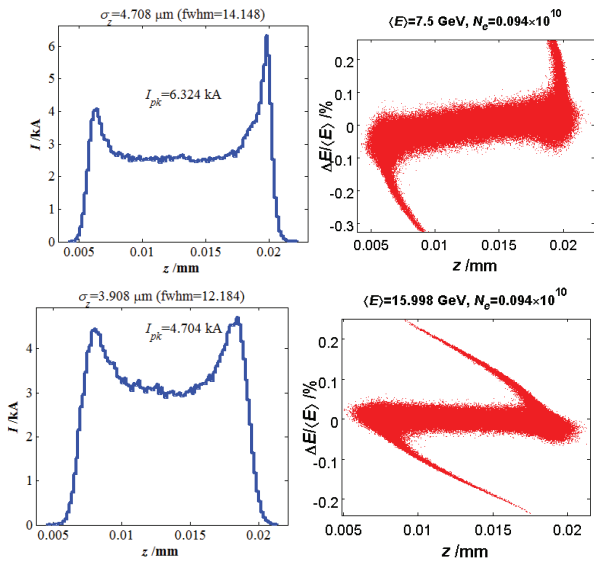
Figure 9: The bunch profile and phase space of low energy beam (top) and high energy beam before the undulator for 150pC beam. Bunch head is on the left.
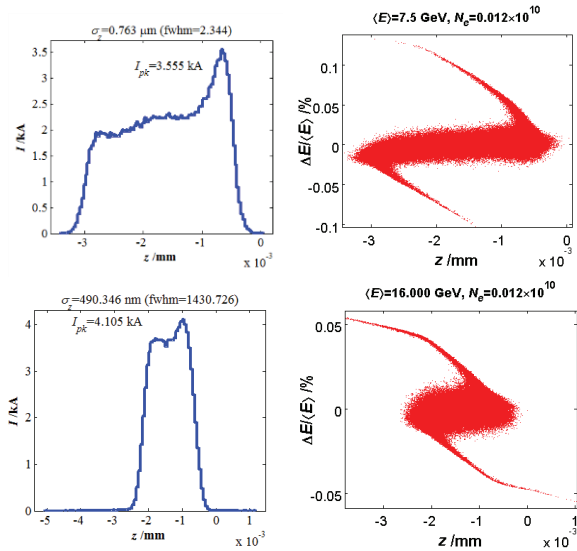


Figure 10. The bunch profile and phase space of low energy beam (top) and high energy beam before the undulator for 20pC beam

## MINIMIZATION OF EMITTANCE GROWTH DUE TO CSR

The collective effects, i.e. space charge (SC) forces, geometric wake fields in the accelerating structures and the coherent synchrotron radiation (CSR) emission in dispersive systems, can induce projected emittance growth. Among them, the CSR effect can be minimized by a better design. The energy modulation and transverse emittace excitation induced by CSR in different dispersion sections can be canceled [2-4] or moderated with an appropriated design of the optics.

There are four dispersion sections in LCLSII, two bunch compressors, Dog-Leg-2 and HBEND section. Figure 11 shows the Twiss functions and dispersion along the hard x-ray beam line. Since both beam and optics are

different in these dispersion sections, there is no perfect cancellation of CSR effect. To minimize the final transverse emittance before the undulator, a virtual phase shifter before HBEND dispersion section is added. Furthermore, we assume that both the horizontal and vertical phase can be adjusted independently. The simulations have been done with ELEGANT code [5]. Fig. 12 shows the dependence of the emittance at the beginning of the undulator on the phase shift for the case of 250 pC charge hard x-ray beam. There is a maximum horizontal emittance of 3.4 μm and a minimum one of 1.09 μm at 167.5°. While there is weaker dependence of the vertical emittance on the vertical phase as expected. Fig. 13 shows the growth of the projected emittance along the LCLSII beam line. The cancellation is clear seen with the optimized solution. Studies with different charge show the optimized phases are slightly different.
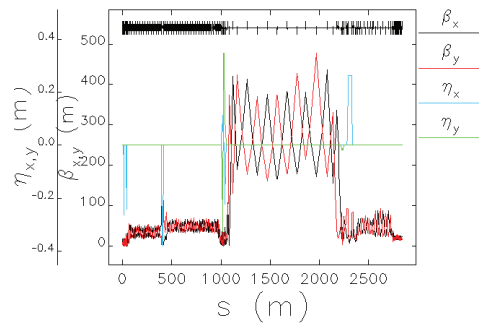


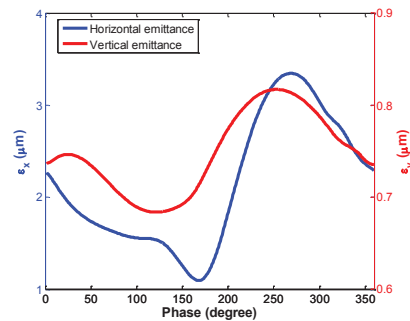Figure 11: Twiss functions and dispersion along the Hard X-Ray beam line.



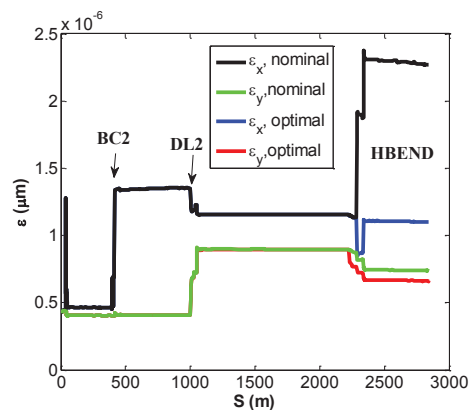Figure 12: Effect of phase shift on the emittace at the beginning of the Undulator for 250pC Hard X-ray beam.



Figure 13: The growth of emittance along the hard X-ray beam line with 250 pC beam.

## SUMMARY

MOGA is applied to optimize the LCLSII, LCLS and LCLSII+ in order to minimize the jitters, energy spread and energy chirp. Small energy spread, zero energy chirp and small jitter are achieved for different bunch charge. MOGA provides a very useful tool in the design. Our preliminary study shows that the energy jitter in LCLS can be reduced by a factor of 2 by optimizing the machine configuration. LCLSII+ can provide two beams with different energies simultaneously and with large flexibilities in beam energy, bunch charge and energy chirp.

The emittance growth due to CSR can be minimized by simply choosing an appropriate phase advance between BC2 and DL2 or LTU. The optimal horizontal emittance is about 1.1 μm and 0.3μ m for 250 pC and 40 pC case. The emittance can be further minimized by reducing the betatron function at BC2.

An integrated Start-to-End (S2E) optimization is desired to further optimize the injector and Undulator.

## ACKNOWLEDGEMENTS

## REFERENCES

[1] F.-J. Decker, et. al., FEL2013, (New York, NY, 2013) WEPSO10

[2] S. Di Mitri, et. al., Phys. Rev. Lett. 110, 014801 (2013)

[3] D. Douglas, Thomas Jefferson National Accelerator Facility Report No. JLAB-TN-98-012, 1998.

[4] E. D. Courant and H. S. Snyder, Ann. Phys. (N.Y.) 3, 1 (1958); See also S.Y. Lee, Accelerator Physics (World Scientific, Singapore, 2007).

[5] M. Borland, et al., TH6PFP062, PAC 2009, Vancouver, BC, Canada.